Chapter 5

Magnetic-ordering of epitaxial Yttrium Iron Garnet thin film

Abstract

YIG is primarily grown on the GGG substrates because of the minor difference between the lattice parameters of these two. However, the previous chapter presents the YIG/SiO_2 to evaluate the potential of the present growth method; this chapter bridges that gap and presents the YIG grown on the GGG substrate using the sol-gel-based spin coating. The GGG single crystal of the lattice parameter 12.379 ± 0.012 Å is used as the seed layer to grow the stressed epitaxial YIG thin film of the thickness 18 ± 1 nm. This film has been studied extensively using the GIXRD, XRR, AFM, XPS, and FMR. The XRR-based surface roughness observed in this method is 0.5 ± 0.1 nm with the higher stress-induced interfacial roughness of 0.8 ± 0.1 nm. This interfacial stress results in the stress-induced anisotropy constant (K_σ) of 4.4 ± 0.002 kN/m^2 that was a significant contribution of the total anisotropy K of 4.7 kN/m^2 present in the grown thin film.

5.1 Introduction

Sol-gel-based spin-coating is an all-solution method that requires nitrates and acetates to make a solution. In the case of yttrium, nitrates are low-priced compared to oxides used as precursors for forming targets in PLD and rf-sputtering. Sol-gel-based spin-coating is a cost-effective method that can be utilized to deposit various oxides [45, 50, 124]. Since the discovery of YIG, it has shown its potential with magnon propagation, magneto-optic behavior, its application as oscillators, and as a key material to study the magnon behavior [164, 180, 181, 30, 182, 183, 184]. The propagation length of magnons is a few mm in μm thick YIG [185, 81, 186]. YIG is an ideal conduit for magnon propagation-based applications and studies of spin pumping and spin magnetoresistance [187, 188, 150, 189, 190, 191, 192]. YIG has a unit cell comprised of 160 atoms with the three kinds of coordination, i.e., tetrahedral, octahedral, and dodecahedral sites of Fe^{3+} and Y^{3+} cation [193, 194]. Fe^{3+} cations are present in octahedral and tetrahedral sites. The ratio between the two is 2:3, respectively. Then there is the presence of superexchange in the Fe^{3+}-O^{2-}-Fe^{3+} bonds, and the Goodenough-Kanamuri rule states the presence of the antiferromagnetic coupling between the two half-filled Fe^{3+} cations [59]. This coupling is between unbalanced number of Fe^{3+} cations, giving rise to the ferrimagnetic behavior of the YIG. These ferrimagnetic materials have shown their potential in evolving spintronics and magnonics [195, 147, 196, 197, 198, 80, 199]. YIG, in practice, is deposited using the LPE, PLD, and rf sputtering [200, 201]. Sol-gel-based deposited epitaxial YIG needs to be addressed in the literature. In a few works of literature, the sol-gel-based spin-coating has been reported for deposition of the polycrystalline YIG/Si [45, 161, 202].

This chapter presents the YIG/GGG(111) epitaxial growth using sol-gel-based spin coating. The structural, topography, stoichiometry, and magnetic properties of YIG with the sol-gel-based spin coating are discussed comprehensively. The strain in the thin film is due to the

lattice mismatch, which is well established in the literature [63, 203]; a similar behavior is observed with the sol-gel method here. This shows that stress-induced magnetic anisotropy significantly contributes to the magnetic anisotropy in the epitaxial YIG/GGG thin film and the magnitude of the anisotropy similar to the PLD-grown thin films.

5.2 Results and Discussion

5.2.1 Structural Study

The thin film of YIG was deposited on the single crystal GGG. XRD was utilized to confirm the epitaxy and the phase of the YIG/GGG. Initially, lab XRD was performed using CuK_{α} of the wavelength 1.5406 Å. But the presence of $K\alpha_1$ and $K\alpha_2$ X-ray lines hinder the resolution of the YIG peak. Therefore, monochromatic synchrotron GIXRD has been utilized with the wavelength 1.235 Å. Highly monochromatic radiation gives the distinguishing peak of YIG. Figure (5.1) depicts the GIXRD of the YIG thin film. The GIXRD shows the highest intensity substrate peak of GGG (444) reflection, with the broad YIG (444) Bragg reflection. The Laue oscillation in the GIXRD confirms the high crystallinity with excellent interface roughness. The (444) reflection of the GGG and YIG were observed at 2θ are 40.437° and 40.7°.

The YIG and GGG crystal structure is cubic with the space group $Ia\bar{3}d$. The Bragg's equation:

$$2dsin\theta = n\lambda \tag{5.1}$$

where, d is interplanar distance, θ is angle of reflection, and λ is wavelength used. Considering the d value from the above equation and substituting it with the following equation:

$$d = \frac{a}{\sqrt{h^2 + k^2 + l^2}} \tag{5.2}$$

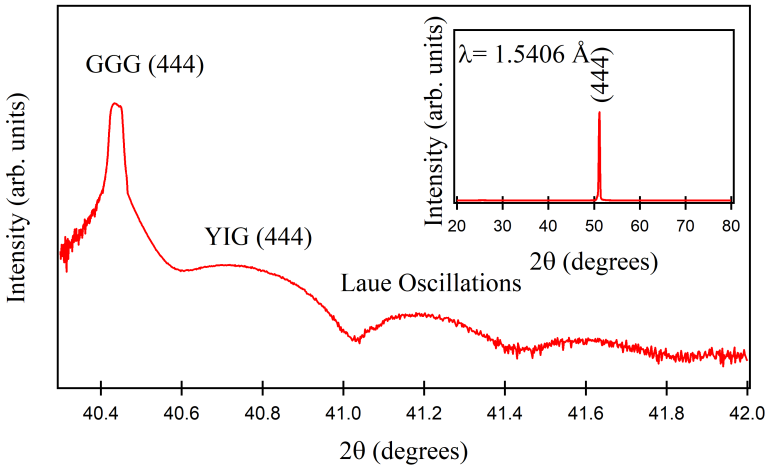

Fig. 5.1 *Synchrotron GIXRD of (wavelength 1.235 Å) the epitaxial YIG with Laue oscillations for excellent crystallinity. Inset shows the Lab XRD showing (444) reflection of GGG.*

The lattice parameter estimated with the above equation for GGG (a_{GGG}) and YIG (a_{YIG}) was 12.379 $\pm$ 0.012 Å, and 12.302 $\pm$ 0.012 Å, respectively. The GGG (111) lattice parameter in literature was 12.383 Å, and the reported value in this work with the error bar was also accordingly [63, 204, 205]. The a_{YIG} was smaller than the literature in which the value of the lattice parameters ranges from 12.363 - 12.467 Å [63]. The lattice parameter was reduced compared to the bulk value (12.376 Å) because of the quenching of the thin film. The thermal expansion coefficient of the GGG and YIG is 1.08 $\times$ 10^{-4} Å/ K and 1.29 $\times$ 10^{-4} Å/ K, respectively. As the thin film was quenched in the air, the surfaces got a higher quenching rate, and the YIG had a higher thermal expansion coefficient, resulting in the shrunken YIG lattice parameter. This case is the opposite of the PLD-grown samples at high temperatures, where the substrate is heated while the deposition and further annealing are done, followed by the cooling at lower rates; the difference arises because of the quenching process in this work. To understand it better, the lattice mismatch is estimated

using the formula given below [63]:

$$\Delta\varepsilon = \frac{a_{GGG} - a_{YIG}}{a_{GGG}} \tag{5.3}$$

The substrate and thin film mismatch $\Delta\varepsilon$ = 0.61%, which was comparable with the PLD-grown samples in the literature, where the value of $\Delta\varepsilon$ ranged from 0.1 - 0.7% (values are absolute) [63]. $\Delta\varepsilon$ depicts the compressive strain in the thin film. The present reported strain is similar to thin film grown at 800 °C followed by the annealing for 2 hrs at 800 °C in work by Bhoi et al. [63]. Despite the shrinking order being similar to the PLD-grown samples, the reference point of the strain here was the initial YIG lattice parameter in this work, opposite of the GGG reference point in the PLD-grown samples. The argument presented that quenching shrunken the lattice parameter and higher thermal expansion coefficient YIG shrunken more comparing the GGG, which is valid, as the strain is similar to literature at similar substrate and growth conditions. Utilizing the mismatch of the YIG and GGG, the stress is estimated using the below equation [64]:

$$\sigma = \frac{Y}{1-\nu}\Delta\varepsilon \tag{5.4}$$

where, the ν is Poission's ratio, and Y is Young's modulus. The value of the ν is 0.29 and Y is 2.00×10^{11} N/m^2 as present in literature [206]. The estimated value of the σ is 1.7 $\pm$ 0.0014 $\times10^9$ N/m^2, within the range of the stress reported in the literature [63]. The presence of stress in the system causes magnetic anisotropy due to the magneto-elastic contribution as the growth is in (111) direction and considering the magnetostriction constant $\lambda_{(111)}$ = -1.7$\times10^{-6}$ from the literature [63, 65]. Substituting the stress (σ) and the magnetostriction constant, the stress-induced anisotropy has been calculated using the following equation:

$$K_\sigma = -\frac{3}{2}\lambda_{(111)}\sigma \tag{5.5}$$

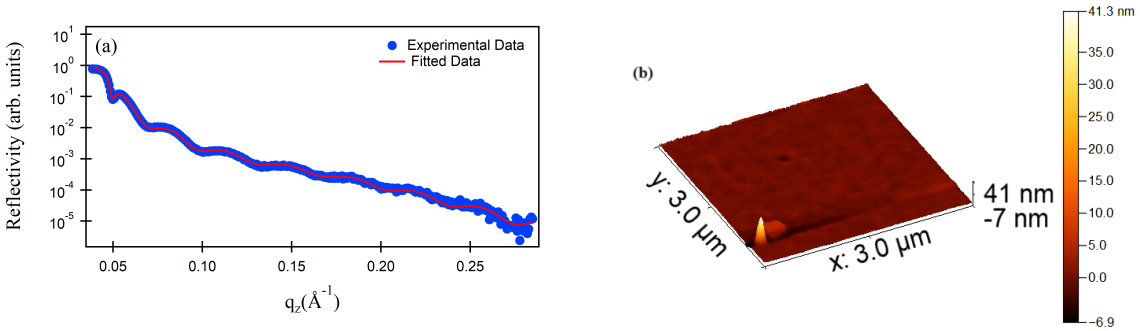

Fig. 5.2 *The thickness analysis of the epitaxial YIG utilizing the XRR and the topography study utilizing the AFM.*

The estimation of the K_σ is 4.4 $\pm$ 0.002 kN/m^2 which is positive and contrary to the literature where higher negative K_σ of the magnitude 0.5 kN/m^2 is presented for the similar annealing temperatures [63]. The sign difference is because of the shrinking of the YIG lattice, compared to the relaxed lattice parameter in the literature for similar growth temperatures [63].

5.2.2 Thickness and Topography Study

A non-destructive method to estimate the thickness of the thin film is XRR, which allows an estimate of the YIG/GGG's thickness, surface, and interfacial roughness of the YIG/GGG [207, 163]. Figure (5.2)(a) presents the experimental and fitted XRR data of the YIG with the (b) AFM image of the epitaxial YIG. The experimental XRR data is fitted using Parratt's formulism utilizing the Parratt32 software [110, 208]. The χ^2 was measured using the formula (log(R_{exp})-log(R_{fit}))^2 results into the value 5 $\times$ 10^{-3} as per the best fit. The thickness estimation suggests the presence of an interfacial layer of Gadolinium iron garnet (GdIG); evidence of such an interface is present in the literature [209]. The thickness observed using the XRR of YIG was 17 $\pm$ 1 nm with the interfacial GdIG of 1.2 $\pm$ 1 nm. The surface roughness is $\approx$ 0.7 $\pm$ 0.1 nm, and the interfacial roughness is 0.8 $\pm$ 0.1 nm. The laue oscillation in the GIXRD also confirms the excellent crystalline quality

of the deposited YIG sample. The topography of the YIG is depicted utilizing AFM. The estimated surface average roughness is 0.6 ± 0.1 nm, the same order as the XRR. The AFM suggests the primarily homogeneous growth of the YIG on GGG(111) with some large spikes and troughs mostly at the edges because of the crystal growth nature of the thin films [210]. These spikes result from some impurity centers, giving rise to a higher growth rate at certain points [211]. Troughs are observed at the edges mostly because of the edge non-uniformity of the spin costing.

5.2.3 Elemental and Ionic Environment Study

The confirmation of the stoichiometry was performed utilizing the XPS. Figure (5.3)(a) depicts the survey scan of the thin film. Oxygen, iron, yttrium, and carbon in the survey scan have been identified. Calibration was performed considering C_{1s} at a binding energy of 284.8 ± 0.1 eV.

Figure 5.3(b) depicts the oxygen anion's high-resolution spectrum. The thin film contribution is at a binding energy of 529.3 ± 0.1 eV, and the surface hydroxyl oxygen is at a binding energy of 531.6 ± 0.1 eV. Figure (5.3)(c) depicts the high-resolution spectrum of the Y_{3d}. The peak positions of $Y_{3d_{5/2}}$ and $Y_{3d_{1/2}}$ at binding energies of 156.9 ± 0.1 eV and 158.9 ± 0.1 eV. These follow the literature and present Y^{3+} cationic state [50].

Figure (5.3)(d) depicts the high-resolution spectrum of the Fe_{2p}. The deconvoluted high-resolution spectrum shows the presence of two peaks in each $Fe_{2p_{3/2}}$ and $Fe_{2p_{1/2}}$. The two constituents are because of the two Fe cation environments. Fe cations are present in tetrahedral and octahedral coordinates. The four oxygen anions surround the tetrahedral, and six oxygen anions surround the octahedral. As the crystal structural study confirms the presence of two octahedral Fe_{octa} and three tetrahedral Fe_{tetra}, the ratio between the two is

2:3 [166]. The peak of $Fe_{2p_{3/2}}$ is at 709.8 ± 0.1 eV and 711.6 ± 0.1 eV for the tetrahedral and octahedral coordination, respectively.

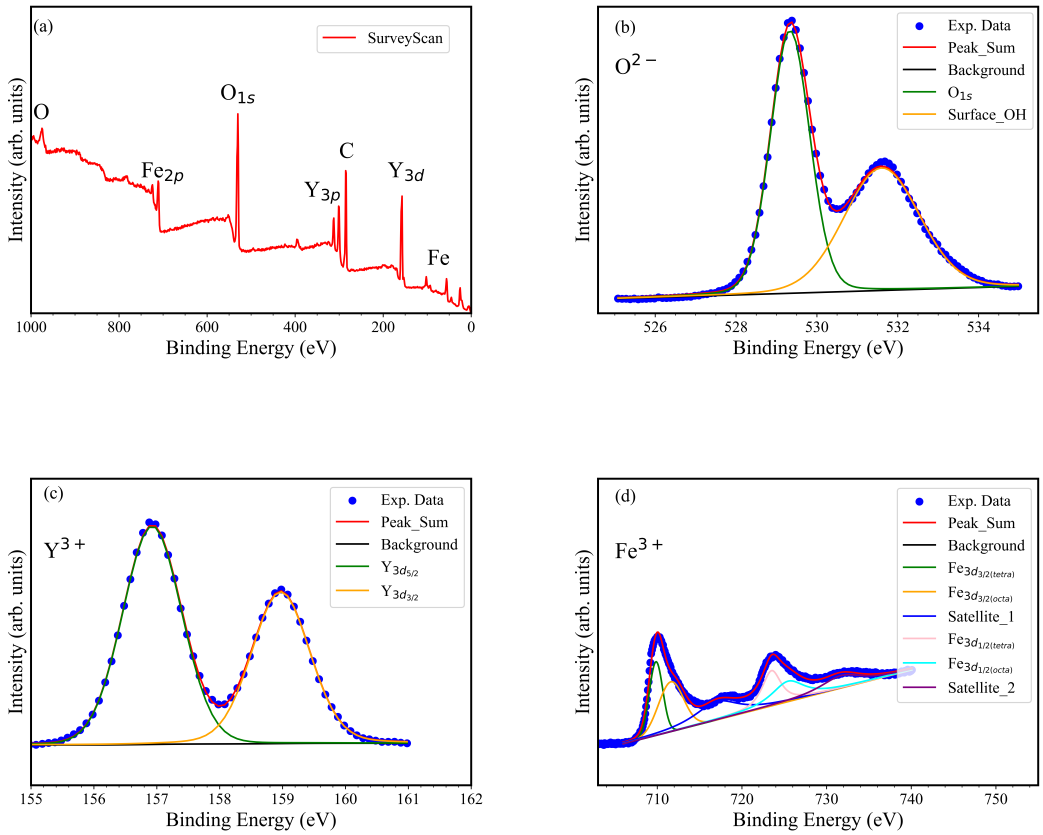

Fig. 5.3 *(a) Survey scan of the YIG/GGG sample depicts the presence of elements Fe, O, Y, and C on the surface. High-resolution spectrum of the (b) O^{2-}_{1s}, (c) Y^{3+}_{3d}, and (d) Fe^{3+}_{2p} is deconvoluted.*

The peak of $Fe_{2p_{1/2}}$ is at 723.5 ± 0.1 eV and 725.4 ± 0.1 eV for the tetrahedral and octahedral coordination, respectively. The presence of a satellite peak at a difference of ≈8 eV from the tetrahedra peak confirms that the cationic state of iron is 3+. To confirm the crystallographic ratio between octahedral and tetrahedral Fe, experimentally, the intensity of the Fe_{octa}: Fe_{tetra} are calculated. The experimental ratio for the $Fe_{2p_{3/2}}$ is 0.66 and $Fe_{2p_{1/2}}$ is 0.56. $Fe_{2p_{1/2}}$ which slightly deviates from the expected value because of the

assumption of a linear background. The atomic percentages of oxygen, iron, and yttrium are estimated using CASAXPS software, and the estimation is 55.7%, 25.0%, and 19.3%, respectively [169]. The experimental atomic percentages are close to the estimation of stoichiometry, i.e., 12:5:3 for the O:Fe:Y ratio.

5.2.4 Magnetic Study

The magnetic behavior of the epitaxial YIG thin film was studied using the FMR at room temperature [212, 213]. The field-dependent data were taken in the 2 GHz to 12 GHz frequency range. Figure (5.4)(a) depicts FMR spectrum from 2 - 12 GHz frequency as a function of varying magnetic field. The primary peaks are the uniform excitation of the magnetization in the formula unit [18]. However, it is evident in AFM that spikes and troughs are present in the epitaxial YIG thin film. These spikes and troughs result in secondary peaks alongside the uniform excitation. In literature, the theoretical studies present evidence of the formation of the standing wave with uniform excitation because of the anti-dots; in the present work, these perturbations are troughs and spikes [214]. Figure (5.4)(b) the frequency as a function of the H_{res} is plotted and fitted using the Kittel equation. The magnetic field is applied in the plane. The Kittel equation for the in-plane magnetic field on thin film is as follows:

$$f = \left(\frac{\gamma}{2\pi}\right)\sqrt{H(H+\mu_0 M_{eff})} \tag{5.6}$$

where, f is applied frequency, γ is a gyromagnetic ratio, and $\mu_0 M_{eff}$ is the effective magnetization. Figure (5.4)(b) depicts the experimental data and the Kittel fitted frequency as a function of resonance field. The value of the gyromagnetic ratio is 28.49 $\pm$ 0.05 GHz/T, and the g-factor was estimated as 2.05 $\pm$ 0.007. The fitted curve gives the estimated $\mu_0 M_{eff}$ = 0.05 $\pm$ 0.002 T which was less than the saturation magnetization (M_S) indicating

the presence of the anisotropy in the YIG/GGG thin film. The relation between the $\mu_0 M_{eff}$, M_S and anisotropy field is as follows [215]:

$$\mu_0 M_{eff} = \mu_0 M_S - H_U \tag{5.7}$$

M_S is assumed from the literature, and its value is 0.1382 T. The result of two substitutions gives the H_K = 0.0852 T. This H_K and M_S is used to estimate the anisotropy constant (K)) calculation as per the below equation:

$$K = \frac{H_U \times M_S}{2} \tag{5.8}$$

The K is estimated from the above formula is 4.69 kN/m^2. Total anisotropy can be measured by combining cubic anisotropy, shape anisotropy, and stress-induced magnetic anisotropy. The value of the cubic anisotropy in the YIG is -0.57 kN/m^2 and shape anisotropy is 0.605 kN/m^2 with stress-induced anisotropy calculated with equation 5.5. The total anisotropy is estimated as 4.4 kN/m^2 by substituting all in the equation. The difference between the two is 0.29 kN/m^2 because of the approximate value of the M_S from the literature. As the literature presents, the significant contribution of anisotropy is because of the stress-induced anisotropy and very little due to the cubic or shape anisotropy.

Figure (5.4)(c) depicts the damping parameter estimation using the linear fit to the linewidth (ΔH) as a function of frequency. The estimated Gilbert damping parameter $\alpha = 7.6 \pm 0.3 \times 10^{-3}$, which is higher than the polycrystalline YIG, i.e., $4.7 \pm 0.3 \times 10^{-3}$. The increase in the α is because of the GdIG interface [209], whose presence is in the XRR study. As the literature by Kumar et al. presents, the antiferromagnetic exchange coupling between the YIG and GdIG interface causes spin inhomogeneity that contributes to intrinsic damping, which results in the enhanced Gilbert damping constant [209]. The non-homogeneous

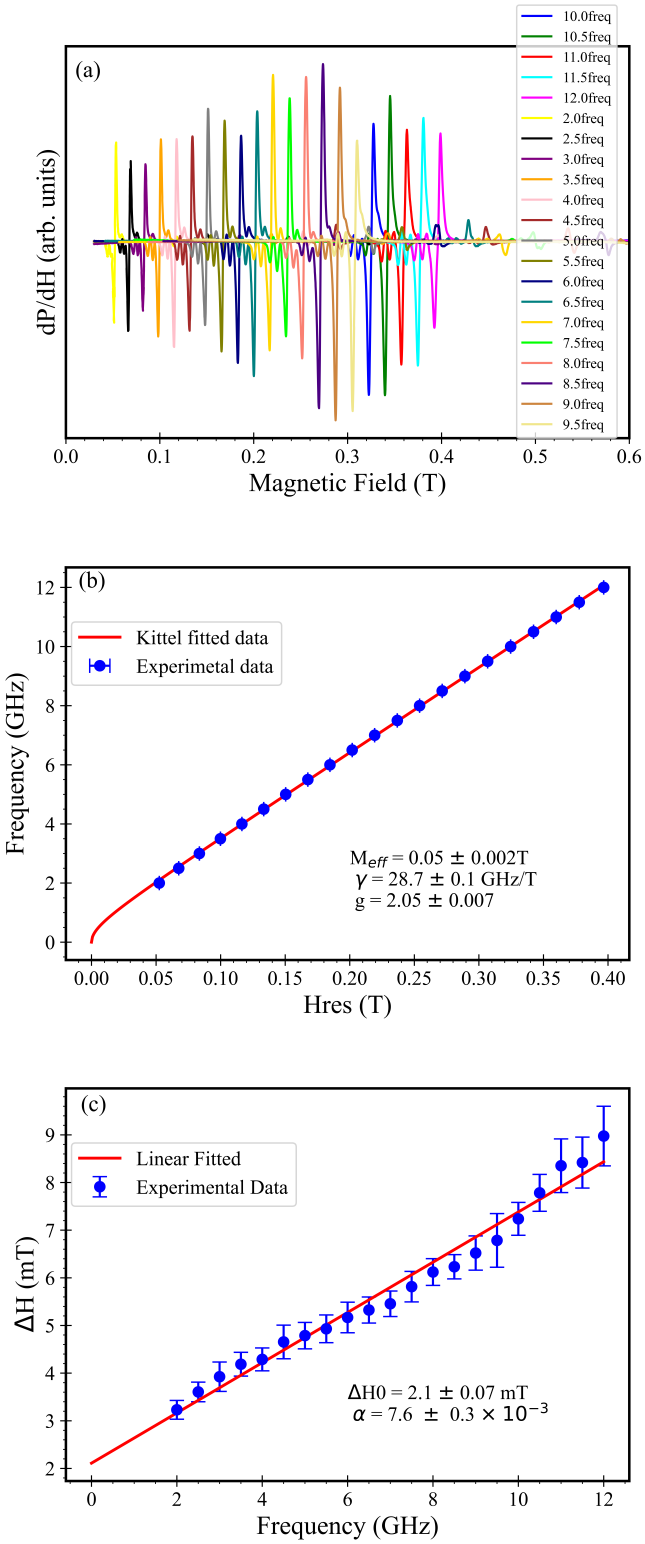

Fig. 5.4 *(a) Derivative of the phase as the function of the applied DC magnetic field of the YIG/GGG sample from frequency 2.0 to 12 GHz (b) Frequency is plotted as a function of resonance magnetic field and fitted using Kittel formula and (c) experimental linewidth (ΔH) has been plotted as a function of frequency and fitted linearly. (The FMR measurement was performed at room temperature.)*

contribution (ΔH_0) to the damping in the epitaxial YIG is 2.1 $\pm$ 0.7 mT. The intrinsic contribution is higher because of the GGG and YIG interface interaction as the epitaxy reduces the defects, and the energy dissipation is due to non-homogeneous contributions associated with the defects[216, 217, 218].

5.3 Summary

The Sol-gel-based spin-coating has the potential to deposit an epitaxial thin film of the $\approx$17 nm YIG on the GGG(111) single crystal. The surface roughness of 0.7 $\pm$ 0.1 nm shows its excellent quality. High crystallinity is confirmed with the GIXRD. The epitaxial YIG has stoichiometry deposition, as demonstrated by the XPS. The magnetic study is performed with FMR, with the enhanced Gilbert damping due to the interfacial antiferromagnetic coupling of the YIG and the GdIG. The FMR study with the XRD study shows anisotropy in the epitaxial YIG. This work estimates the net sum of the stress-induced anisotropy, shape anisotropy, and cubic anisotropy to get the total anisotropy. The significant contribution to the total anisotropy is the stress-induced anisotropy in sol-gel-based spin-coating, as presented in the literature.